Controlled Vortex Formation at Nanostructured Superconductor/Ferromagnetic Junctions

Björn Niedzielski and Jamal Berakdar*

Stability and transport properties of superconducting/insulating/ferromagnetic nanostructures are decisively affected by vortex formation in the superconductor. Herein, the emergence of such vortices due to finite size and geometric effects is studied using a Landau–Ginzburg approach coupled to the magnetic layer via its stray field. Numerical simulations based on the finite-element method evidence that magnetic vortices can be induced and coupled to each others upon appropriate nanostructuring of the magnetic films. These findings are of immediate relevance to transport properties of such structures.

1. Introduction

From a formal, statistical field-theory point view, superconductivity and ferromagnetism share a number of similarities as macroscopic ordering phenomena; the underlying microscopic quantum origin is however different hindering often their coexistence in a single phase: Strong exchange interactions in ferromagnets (FMs), for instance, tend to align electronic spins counteracting the stability of the weakly bound singlet Cooper pairs in a conventional superconductor (SC). This type of incompatibility is, in contrast, advantageous when it comes to interface effects in layered SC/FM structures that relay on a nanoscale proximity coupling. Nanostructuring and confinement effects bring in further interesting phenomena such as the formation and shaping of superconducting vortices, and on the FM side, magnetic domains, FM vortices, or other topological FM states may emerge. Advances in the fabrication and characterization of FM/SC hybrid structures made possible a detailed investigation of ferromagnetism and superconductivity in close proximity and led to rapidly increasing research activities with a series of possible and realized applications. A plethora of new effects have been discovered or predicted, e.g., the enhanced pinning of vortices by lattices of magnetic dots,[1–3] vortex–antivortex (vav) molecules,[4] magnetoelectric effects,[5–8] skyrmion–vortex interaction,[9–11] magnon–vortex interaction,[12–15] vav crystals,[16,17] domain-wall superconductivity,[18,19] to name just a few. The control of vortex dynamics and effective pinning are crucial for applications where high-current densities are needed, as well as magnetoresistance phenomena in SC/FM junctions. It has been shown by numerous theoretical and experimental studies that the inhomogeneous field of a FM close to a SC can significantly change the critical properties of the adjacent SC.[20,21] Another consequence of the ferromagnetic stray field is the emergence of antivorticies and vortex loops.[22,23] The two order parameters may directly couple at the SC/FM interface but even if the FM is separated from the SC by a thin insulating layer, the stray fields of the finite or/and structured FM layer may affect the ordering in the SC layer. Furthermore, as established for mesoscopic SCs, the spatial extent and the geometry of the SC sample are important factors that influence significantly the vortex behavior.[24–26] Demagnetizing effects and the requirement for no supercurrent leaving the SC in conjunction with a curved geometry lead to many fascinating phenomena such as the emergence of gigant vortices[27] or the current-driven formation of vav-pairs.[28] In this work, we demonstrate how the inhomogeneous stray field of a multi-domain FM acts on finite-size, mesoscopic SC. Special attention is paid to the formation of vortices due to the proximity of the FM layer. Vortices in two different SC layers maybe effectively coupled to each other via the stray field of the FM layer. The phenomena discussed in the work are well described by solutions of the time-dependent Ginzburg–Landau equations of superconductivity (TDGL) with the method of finite elements. This allows to account for demagnetizing effects and vortex confinement in finite geometries under realistic conditions. A finite-size FM may have several FM domains and inhomogeneous stray fields which we found may lead to the creation of different vav-states in the SC. The back action of the particular ordering in the SC on the FM state is, in general, very weak and is not discussed in this work. In fact, we study FMs that are sufficiently hard not to be affected by external magnetic fields or the fields produced by the SC.

B. Niedzielski, Prof. J. Berakdar
Institut für Physik
Martin-Luther Universität Halle-Wittenberg
Halle 06099, Germany
E-mail: jamal.berakdar@physik.uni-halle.de

The ORCID identification number(s) for the author(s) of this article can be found under https://doi.org/10.1002/pssb.201900709.

2. Theory and Simulation Details

We consider a system consisting of a Nb film on top of a FM (cf. **Figure 1**). For a clear understanding of both materials, we focus on a square film geometry with a side length $a = 2\,\mu m$ and a thickness of $d = 200\,nm$. The two materials are separated
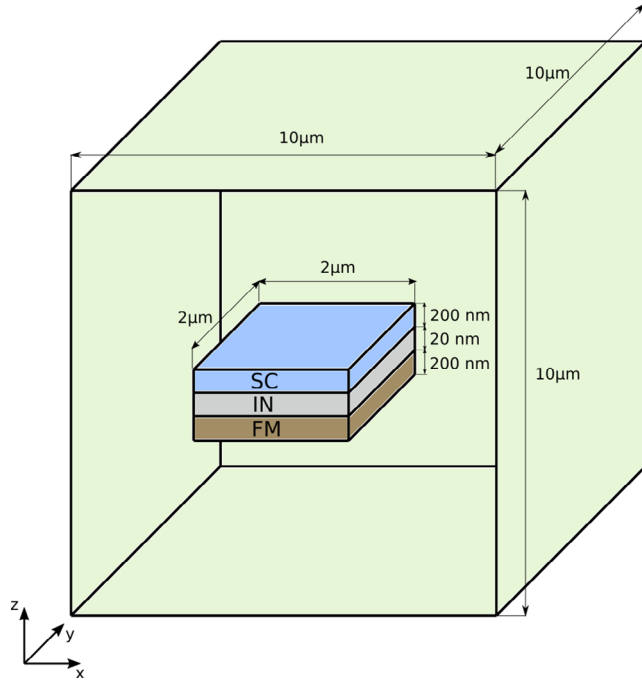
Figure 1. Sketch of the considered system. The SC and FM are thin square films separated by an insulating oxide layer. The surrounding empty box is necessary to comply with the open boundary conditions for the vector potentials.

by an insulating barrier of thickness $h = 20\,\text{nm}$ to prevent direct proximity effects. Thus, in our case, the interaction is purely electromagnetic. In all presented calculations, the thickness d of each layer as well as their separation distance h are unchanged. In the numerical simulations, we surround the bilayer by a vacuum box. We observe, due to the stray fields of the FM, vortex formation in the SC is enabled under realistic conditions. Also, the appearance of antivortices is possible because the stray fields are highly inhomogeneous in space. For simplicity, the back action from the SC onto the FM is not taken into account. The whole system is held at a constant temperature of $T = 8.1\,\text{K}$, which is close to the critical temperature of bulk Nb $T_c = 9\,\text{K}$. Furthermore, the static magnetization of the FM is chosen as appropriate to the simulation conditions. The SC is simulated by solving the TDGL which in dimensionless form are

$$\eta_1 \frac{\partial \Psi}{\partial t} + i\kappa\phi\Psi + \Psi(|\Psi|^2 - 1) + \left(\frac{1}{i\kappa}\nabla - \mathbf{A}\right)^2 \Psi = 0 \tag{1}$$

$$\nabla \times \nabla \times \mathbf{A}_{\text{sc}} = -\eta_2\left(\frac{\partial \mathbf{A}}{\partial t} + \nabla\phi\right) + \mathbf{j}_\text{s} \tag{2}$$

$$\mathbf{j}_\text{s} = \frac{i}{2\kappa}(\Psi\nabla\Psi^\star - \Psi^\star\nabla\Psi) - |\Psi|^2\mathbf{A}. \tag{3}$$

Ψ is the wave function of the Cooper pair condensate with $|\Psi|^2$ representing the local superconducting density. The electrochemical potential ϕ is eliminated by choosing the gauge $\phi = 0$. Under the conditions outlined above, the interactions between the SC and the FM are mediated by the vector potential $\mathbf{A} = \mathbf{A}_{\text{FM}} + \mathbf{A}_{\text{sc}} + \mathbf{A}_{\text{ext}}$. Here $\mathbf{A}_{\text{FM}}$ is the vector potential

associated with the magnetization vector field of the FM layer and follows from Ampére's law

$$\nabla \times \nabla \times \mathbf{A}_{\text{FM}} = \eta_3\nabla \times \mathbf{M} \tag{4}$$

Magnetic fields from external sources contribute with the vector potential $\mathbf{A}_{\text{ext}}$, and the magnetic fields due to Meißner screening currents in the SC lead to $\mathbf{A}_{\text{sc}}$. The constants η_1 and η_2 are set by the normalization of the TDGL. Time is measured in units of $\tau = 3\hbar^2/2m_\text{s}v_\text{f}l$, length in units of the magnetic penetration depth λ, Ψ in units of $\sqrt{m_\text{s}/\mu_0\lambda^2q_\text{s}^2}$, $\mathbf{A}$ in units of $\sqrt{2}B_{\text{cth}}\lambda = \hbar\kappa/q_\text{s}\lambda$, and $\mathbf{M}$ in units of $M_0 = 1\,\text{kA}\,\text{m}^{-1}$. The coefficient η_2 contains the electrical conductivity in the normal state σ which has a finite value inside the SC and vanishes everywhere else. For the solution of Equation (1) and (2), we use typical material parameters for Nb, as shown in **Table 1**.[29,30] For the TDGL, the usual boundary conditions apply which ensure that $\mathbf{j}_\text{s}$ has no component normal to the boundary of the superconducting domain, and the field of the SC $\mathbf{B}_{\text{sc}} = \nabla \times \mathbf{A}_{\text{sc}}$ tends to zero at large distances.

For the solution of Equation (1)–(4), the finite element package FENICS[31] is used with finite-element meshes generated by the software GMSH.[32] Conventional first-order Lagrange elements are an appropriate choice for the approximation of Ψ and the first-order Nédélec elements for the vector potentials $\mathbf{A}_{\text{sc}}$ and $\mathbf{A}_{\text{FM}}$. The computation domain was discretized into about 10 million tetrahedra with 1 million tetrahedra equally distributed between the FM and the SC.

To find the equilibrium state of the SC for a given magnetization $\mathbf{M}$, Equation (4) was solved for $M = 1\,\text{kA}\,\text{m}^{-1}$ and the resulting vector potential $\mathbf{A}_{\text{FM}}$ was inserted in Equation (1). Having all the external parameters set, the first TDGL can be solved by using a semi-implicit backward-Euler time-stepping scheme.[33] In principle, one could also solve the classic Ginzburg–Landau equation to which Equation (1) reduces when the first two terms are set to zero. However, the resulting nonlinear problem is much more difficult to solve than the time-dependent equation. The use of the TDGL allows to discretize Equation (1) in time and to solve a linear equation in every time step. The solutions found this way then converge toward the equilibrium solution of the classic problem.

During the relaxation process, $\mathbf{A}$ was slowly increased until it corresponded to the field produced by a chosen magnetization $\mathbf{M}$. This procedure is possible because the solution of Equation (4) scales linearly with $\mathbf{M}$. Once the final field value was reached, the relaxation was continued until $\partial_t\Psi < 10^{-3}$. To find the equilibrium state of the SC, it is not necessary to solve Equation (1)

Table 1. Material parameters of Nb and the quantities used in the calculations.

	Quantity	Value
Magnetic penetration depth	λ	266 nm
Ginzburg–Landau parameter	κ	3.4
Basic time unit	τ	3.3 ps
Mean-free path	l	9 nm
Fermi velocity	v_f	$6 \times 10^5\,\text{ms}^{-1}$
Relative temperature	T/T_c	0.9

and (2) simultaneously in every time step. Instead, Equation (1) was solved until a possibly metastable equilibrium was found. The resulting order parameter Ψ was then used to calculate $\mathbf{j}_s$ and $\mathbf{A}_{sc}$ by solving Equation (2) with $\partial_t \mathbf{A}_{sc} = 0$. It is possible to reinsert $\mathbf{A}_{sc}$ in the first TDGL and start the relaxation process again. But, for the results presented here, the field $\mathbf{B}_{sc} = \nabla \times \mathbf{A}_{sc}$ of the SC is rather weak and it does not significantly change the established equilibrium. In our calculation, two relaxation cycles were sufficient to find the simultaneous equilibrium solution of Equation (1) and (2). For the vector potential of the external magnetic fields, the symmetric gauge is chosen $\mathbf{A}_{ext} = -0.5B_0 y \mathbf{e}_x + 0.5B_0 x \mathbf{e}_y$, with B_0 being a constant. This particular vector potential is approximately the field which a SC experiences when placed inside a very long solenoid with homogeneous $\mathbf{B} = B_0 \mathbf{e}_z$ inside. It also corresponds well to the situation in experiments where the SC is placed in the center of a Helmholtz coil.

3. Results and Discussions

Let us consider the case where the magnetic layer consists of two antiparallel magnetic domains as shown in **Figure 2**. We assume a saturation magnetization of $M = 75\,\text{kA}\,\text{m}^{-1}$, which is relatively weak but in the realistic range. For comparison, for Permalloy, $M \approx 600-1900\,\text{kA}\,\text{m}^{-1}$ and Yttrium–Iron–Garnet (YIG) $\approx 140\,\text{kA}\,\text{m}^{-1}$.

There are several reasons to keep the magnetization small. The most important point is that the shape of the FM is reflected in the distribution of its stray fields. This however is apparent only close to the FM. At greater distance from the FM, the field resembles that of an ordinary current loop. To make the geometry of the FM, an important parameter we therefore want to keep is the separation between the SC and FM relatively small. For this reason also the magnetization of the FM should be sufficiently small not to destroy the SC state in the Nb layer. This is especially important for temperatures close to T_c where the upper critical field of the SC is reduced. For sufficiently small separation distance between the materials, the z-component of the stray field will then abruptly change its sign at the borders of the FM as can be seen in **Figure 3**. Also, vortex entry can already be observed at small field values. Furthermore, it was found that a small number of vortices is already sufficient to study the principal behavior of vortices in the displayed nanosystems.

We then calculate for the geometry in Figure 2 the respective fields acting on the SC. The FM and the SC match in size and are perfectly aligned on top of each other, the flux density $\mathbf{B}_M$ resulting from $\mathbf{M}$ has a maximal strength at the bottom edges of the SC as well as along the interface of the two magnets. The thickness of the SC is chosen as $d \approx 2.5\xi$ throughout, with ξ being the Ginzburg–Landau coherence length. In contrast to very thin films, variations of the order parameter can therefore also occur along the thickness of the film. Vortex formation is directly influenced by this additional degree of freedom.
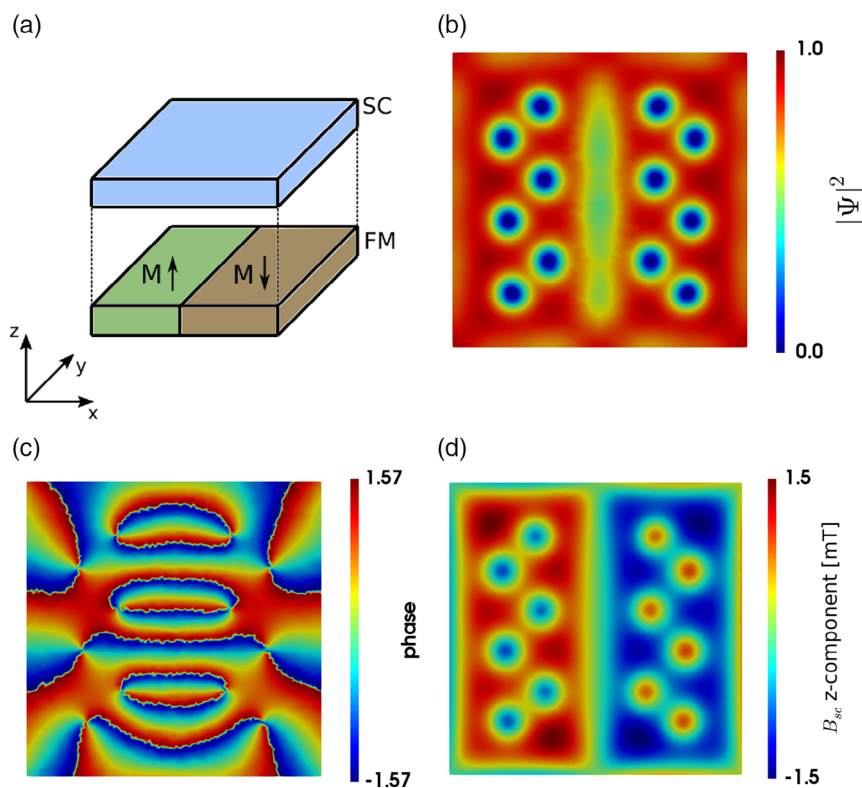

Figure 2. Coupled FM/SC system with two domains with different magnetic ordering in the absence of external magnetic fields. The saturation magnetization is chosen as $M = 75\,\text{kA}\,\text{m}^{-1}$. a) A sketch of the bilayer. b) Cooper pair density $|\Psi|^2$ on a slice through the center of the SC. c) Phase of the superconducting wave function. d) z-component of the flux density B_{sc} on a slice through the center of the SC.
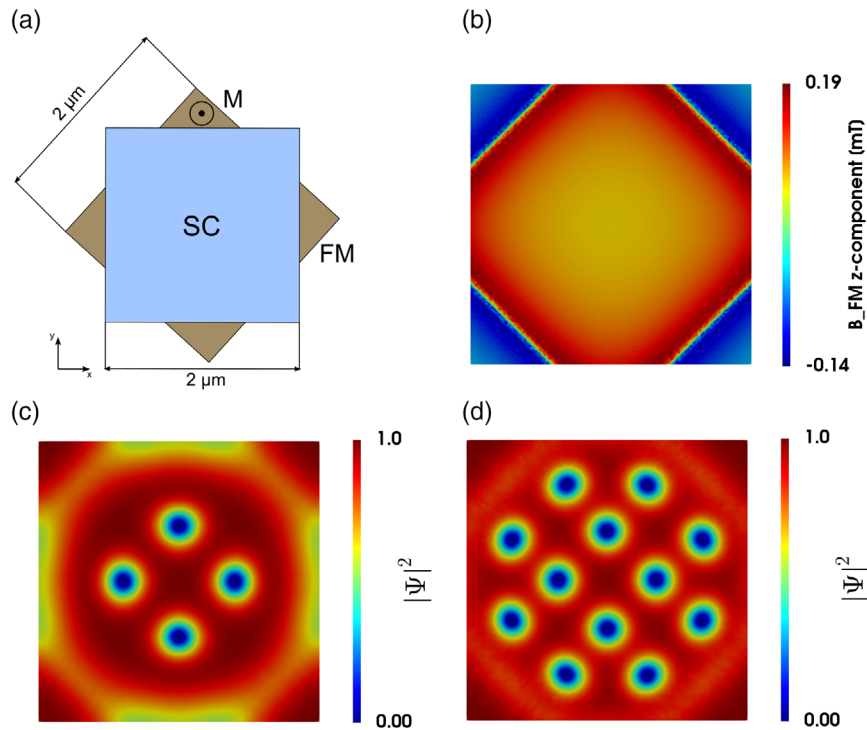
Figure 3. a) FM/SC system with the FM being rotated by 45°. b) Flux density $\mathbf{B}_{FM}$ at the bottom of the SC layer for $M = 1\,\mathrm{kA\,m^{-1}}$. c) Vortex state in the SC for $M = 55\,\mathrm{kA\,m^{-1}}$. d) Vortex state in the SC for $M = 75\,\mathrm{kA\,m^{-1}}$.

In our simulations, it was observed that the vortex formation happens preferentially at the domain wall of the FM, where the stray field has its highest magnitude. Since the total flux in the SC is zero, the vortices always appear in pairs. A single vav-pair evolves from a pocket of reduced order-parameter density at the center of the SC. As this region grows, it splits into two vortex tubes weakly connected to each other and forming a semiloop. Vortex loops and semiloops are typical for extended SCs in the presence of inhomogeneous fields.[34] However, the sample thickness in our case does not allow their stabilization. Instead, vortices and antivortices separate at the domain wall and migrate toward a magnetic domain that stabilizes them magnetically. In this way, two separate subsystems of vortices and antivortices are formed and are magnetically susceptible. The circulating Meißner currents around each domain confine the fluxons and prevent them from mutual annihilation or expulsion from the SC. In this way, a direct vav interaction is prevented.

During the ramp up of the field, it was observed that vortices and antivortices also can enter the SC from the edges. In finite geometries, the edge effects play an important role in the formation and determine the arrangement of vortices. In small SC samples of high symmetry where only a few fluxons can simultaneously exist, it is known that the vortex arrangement follows the sample geometry.[26] Here, we find that in the case of a two-domain magnet, the vortex formation at the edges occurs in multiples of four and in the form of two vav-pairs. The difference between vortices and antivortices is exhibited by their respective phase profile. Around the core of a conventional Abrikosov-vortex, the phase gradient and the corresponding supercurrent circulate around the vortex center. For antivortices, these quantities

circulate in the opposite direction. For this reason, also the flux densities which they generate point in opposite directions.

We also investigated the effect of a static magnetic field $\mathbf{B} = B_0\mathbf{e}_z$ on the FM/SC bilayer. In the absence of the magnetization, such a field leads in an extended SC to population with regular Abrikosov vortices which enter the material from the sample edges. In our case however, due to the strong geometric restrictions, vortices were observed only to appear in multiples of four with the tendency to form a simple cubic lattice instead of a hexagonal one. Two typical lattices created with magnetic fields of $B_0 = 13.5$ and $B_0 = 7.3\,\mathrm{mT}$ are shown in **Figure 4**. The effect of the external field on the FM/SC bilayer was investigated by starting from the fully relaxed state with $M = 75\,\mathrm{kA\,m^{-1}}$ and slowly ramping up B_{ext}. The additional field in the system disturbs the balance of the magnetic flux and introduces an asymmetry in the previously symmetric vav lattices. Fluxons in the region with positive flux experience now a stronger effective field, whereas the field in the region with a negative flux is reduced. Consequently, the lattice of regular vortices shrinks and the antivortex lattice expands. As the field reaches a magnitude of $B_{ext} = 20\,\mathrm{mT}$, the total vorticity in the SC becomes positive as two antivortices are expelled from the domains with negative flux. At the same time, two vortices emerge in the positive flux domain. A further increase in the field strength can fully compensate the stray fields in the domains where antivortices were present, and a homogeneous superconducting state is restored. In the other domain, the superconductivity is strongly reduced because the external field adds to the magnetic stray field. The field compensation in one of the domains also reduces the Meißner currents at the domain wall and the corresponding
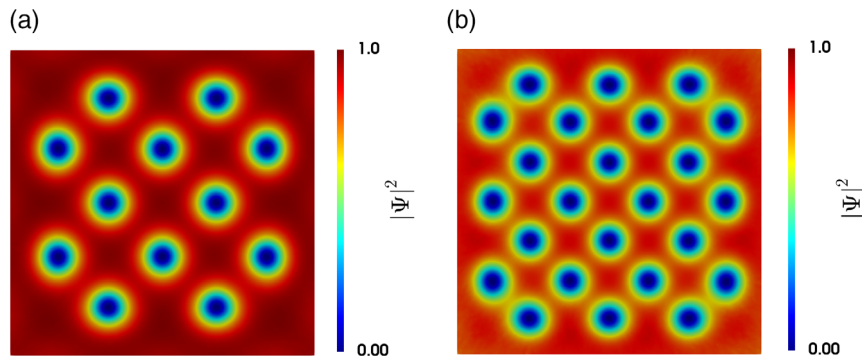
ADVANCED
SCIENCE NEWS
www.advancedsciencenews.com

physica
pss status solidi b
www.pss-b.com

Figure 4. Vortex lattices in the SC for a homogeneous external field $\mathbf{B}_{ext} = B_0\mathbf{e}_z$ with a) $B_0 = 8.5$ mT and b) $B_0 = 15.7$ mT.

strong confining potential for vortices. The vortex lattice can now expand further toward the domain wall until the external field provides a positive flux distribution in the entire SC. The external field was never strong enough to completely remove the confining potential at the domain wall and vav annihilation was not observed in this system.

Similar observations apply to the case of a FM layer structured in four domains on top of which we placed a spacer layer and the SC (cf. **Figure 5**). Here, the adjacent magnetic domains are chosen to have magnetizations pointing in opposite directions, but with equal strength. Experimentally, the FM layer may be made of four plaques with the aforementioned magnetization configuration. We find in this case that above each ferromagnetic domain, an independent vortex/antivortex system is stabilized

for sufficiently strong but realistic magnetization. Vortex entry in these subsystems was again observed to happen at the domain boundaries as well as on the outer sample boundary. The first of these entries leads to the formation of four strictly separated fluxon systems each having two fluxons confined. As the magnetization is increased, more fluxons are forced into the system, but the symmetry of the vav lattices is equal for all field values. It is again possible to disturb the symmetry by applying additional external magnetic fields. In this way, we found it is possible to control the lattice parameter of the fluxons and the fluxon number in each domain. It should be pointed out that in a more realsitic setting, the magnetization may have nonvanishing in-plane components. For this reason, the stray field that acts on the SC is reduced as compared with a complete out-of-plane
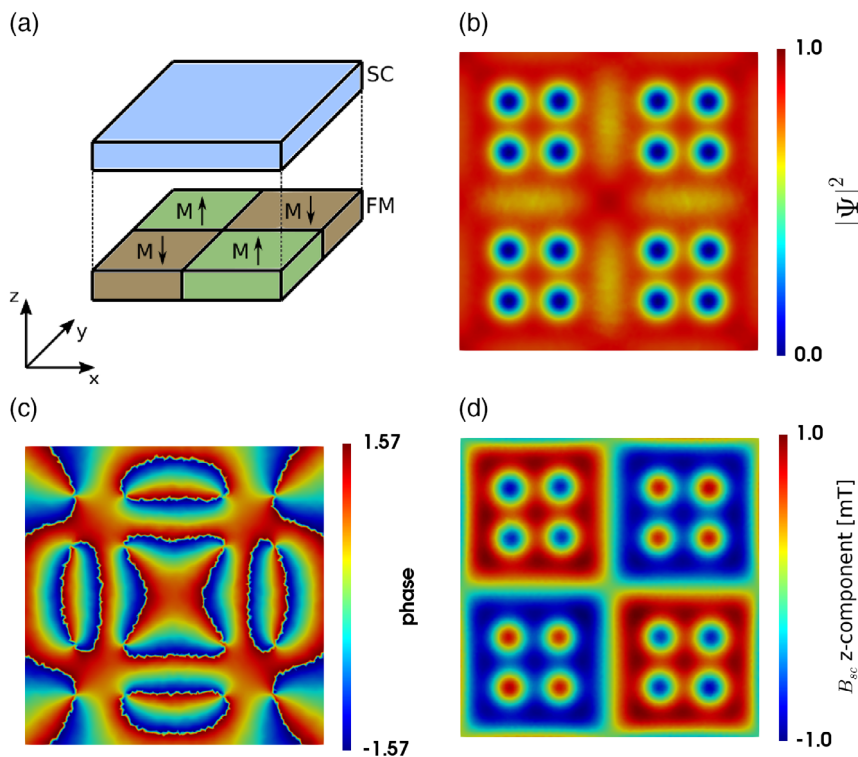

Figure 5. Coupled FM/SC system with four magnetization domains. $M = 95$ kA m^{-1}. No external magnetic field is applied. a) A sketch of the bilayer. b) Cooper pair density $|\Psi|^2$ on a slice through the center of the SC. c) Phase of the superconducting wave function. d) z-component of the flux density B_{sc} on a slice through the center of the SC.

magnetization. Also, the domain width of the FM plays a role in the formation of vav-pairs and should not be neglected.[35,36]

The isolated vortex systems presented here should also be controllable by altering the ferromagnetic domain structure. This fact together with using external magnetic fields offers the possibility to construct nanodevices with easily switchable states represented by fluxons and might be useful as logic devices.[37] Also, the stray field of the vav lattices provides the possibility to control the magnon propagation in coupled FM/SC systems under the combined influence of vav fields.

So far, the geometry of the FM/SC double layer was rather simple with both subsytems having the same size and with both of them being perfectly aligned. To disentangle the effects of geometry and confinement, we change the size and orientation of the FM and also split the SC into disconnected parts that we intend to couple remotely via the stray field of the FM. Every change in the size and the shape of the FM leads to changes in the stray field and therefore affects directly the vortex state of the SC. Starting from the initial setup of the FM/SC layer, the FM is first rotated by 45° without changing its dimensions. A top view of the new geometry with the misaligned FM is shown in Figure 3. In this setup, the z-component of the magnetic stray field in the SC is no longer strictly positive but changes sign at the interface between FM and insulating space outside. As a result, the vortices and the antivortices will again populate areas with the field pointing in the same direction as their corresponding magnetic moment. Since the SC has only a finite size, the flux provided by the FM is not exactly zero and different numbers of vortices and antivortices are possible and expected.

As the field of the FM is slowly increased, vortices appear in multiples of four at the sample edges and travel toward the center. The situation is very similar to the one with a homogeneous field pointing in the z-direction. Also, the vortex lattices are very similar. Structural differences in the vortex arrangement become visible only for higher fields, but still, the overall positive flux dominates the state of the SC and no antivortex has appeared in the simulations. For an infinite SC, the situation would be different because the overall flux in the SC would be zero enforcing the existence of vav-pairs. Therefore, the size of the FM was reduced to make the negative fields more dominant (cf. **Figure 6**). The FM has now only a side length of $a = 1\,\mu m$, but it has the same thickness as before. The stray field in the SC layer is now maximal in the corners of the FM and changes sign abruptly at the FM/vacuum interface. In this system, the negative flux is more dominant, and the vav-pairs are observed to appear in the corners of the FM as the field is increased. However, finite-size effects are still strong, and the emerging antivortices are quickly expelled from the SC. The remaining vortices are gathered in the domain of positive flux. Also, in this system, no antivortex could be stabilized, although their temporary existence was confirmed.

Motivated by this observation, an additional external magnetic field was introduced to this specific FM/SC system. The external field was chosen to point oppositely to the magnetization of the FM to reduce the positive flux distribution at the FM/SC interface and enhance the negative flux outside. The effect of increasing B_{ext} is shown in **Figure 7**. As evident, a sufficiently strong external field can lead to the creation of a stable ring of antivortices around the original vortex arrangement in the center of the SC. This particular vav-system is stabilized by the strong Meißner currents which circulate around the FM/SC boundary and build a magnetic barrier. As the field is further increased, the
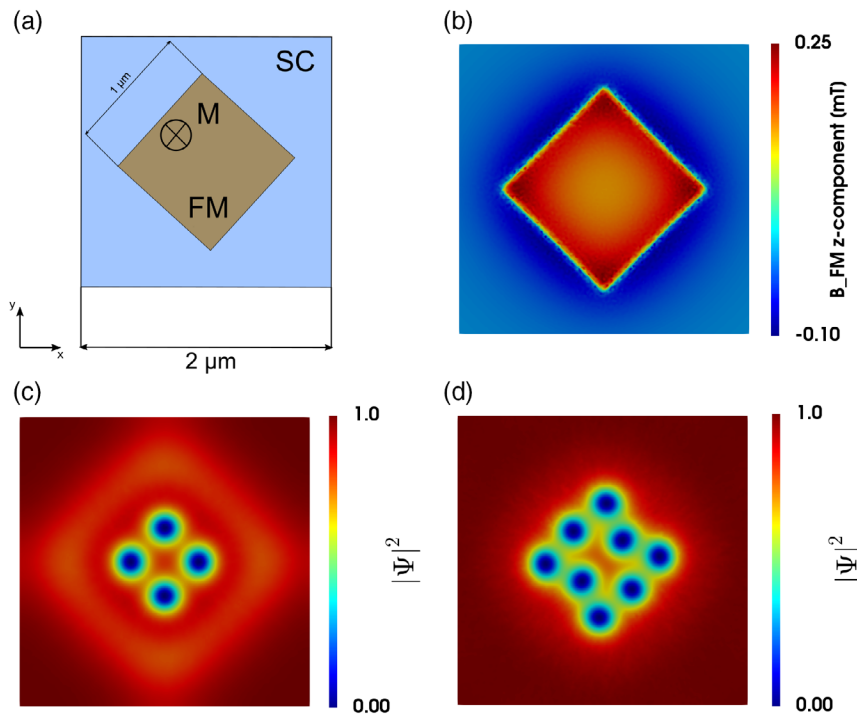

Figure 6. a) FM/SC system with FM rotated by 45° and a smaller side length of $a = 1\,\mu m$. b) Flux density $\mathbf{B}_{FM}$ at the bottom of the SC layer for $M = 1\,kA\,m^{-1}$. c) Vortex state in the SC for $M = 105\,kA\,m^{-1}$. d) Vortex state in the SC for $M = 130\,kA\,m^{-1}$.
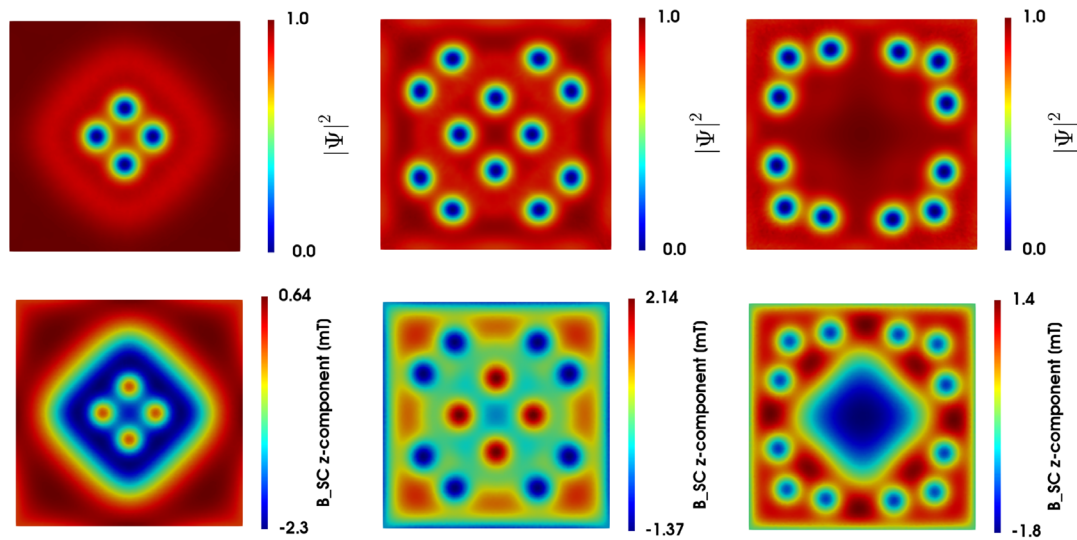
Figure 7. Upper panels: Cooper pair density for the FM/SC system of Figure 6 with $M = 105 \, \text{kA m}^{-1}$. Left: $B_{\text{ext}} = 1.2 \, \text{mT}$, middle: $B_{\text{ext}} = 9.4 \, \text{mT}$, right: $B_{\text{ext}} = 12.3 \, \text{mT}$. Lower panels: flux density B_{SC} of the SC for the same values of B_{ext}, as in the panels above.

strength of the confinement potential is weakened, and the total flux in the SC becomes more negative. For sufficiently strong fields, antivortices can overcome the magnetic barrier and annihilate with the vortices in the center. Again, the field at the FM/SC interface can be neutralized, and superconductivity is locally enhanced. The distribution of Meißner currents at the FM/SC interface strongly depends on the geometry of the FM. Rotating the FM therefore changes the confining potential for the vortices, and the vortex lattice will follow the rotation

which is readily visible by comparing vortex arrangements in Figure 5 and 6. In contrast, the size of the FM controls how the stray fields are distributed and how the vortices and the antivortices will be distributed in the SC.

A further interesting aspect is the shape of the SC that can be changed to manipulate its vortex arrangement. We performed the calculations for a SC split into two independent parts situated on top of the original FM (cf. **Figure 8**), mimicking thus a hybrid SC/FM junction. The main difference to the former cases is that
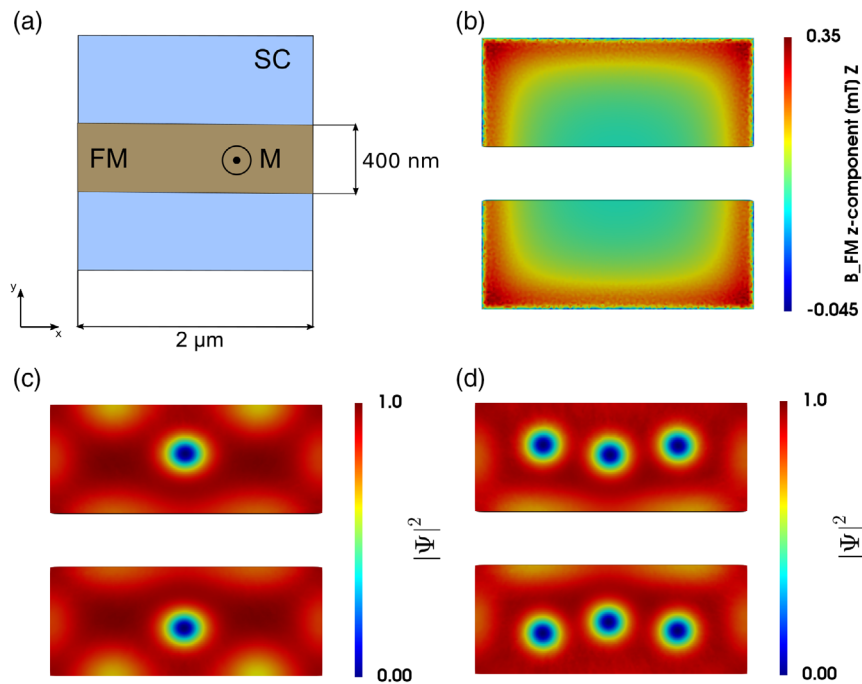

Figure 8. a) FM/SC system with the SC being split into two parts. b) Flux density $\mathbf{B}_{\text{FM}}$ at the bottom of the SC layer for $M = 1 \, \text{kA m}^{-1}$. c) Vortex state in the SC for $M = 65 \, \text{kA m}^{-1}$. d) Vortex state in the SC for $M = 85 \, \text{kA m}^{-1}$.

the two SC have a smaller volume and a rectangular shape. Vortex formation still happens, but the vortex arrangement follows the symmetry dictated by the sample shape. Also, the total number of vortices is smaller for a given field due to the reduced space but with an unchanged vortex–vortex repulsion. We note that despite the existence of two individual SC wave functions Ψ_1 and Ψ_2, the vortex evolution in both SC is not completely independent from each other. The state of each SC is locked to the state of the FM and the interaction is mediated by the ferromagnetic stray fields. In a more realistic model, each SC changes the magnetic state in its vicinity due to its own stray field and has thereby an influence on the other SC. It is again possible to rotate the FM and reduce it in size, but this does not lead to fundamentally new effects, albeit it offers more local control on the modification of the SC order parameters. In none of these cases, antivortices can appear without additional external fields.

4. Conclusion

In mesoscopic SC/FM systems, the formation of vortices and vav nucleation are strongly dependent on the geometry and the size of the constituent materials. The stray field of a well-pinned ferromagnetic state produces stable and symmetric vortex patterns that can be controlled by external magnetic fields. In addition to the stray fields, external magnetic fields allow to control the vorticity in the confined vortex systems and allow to locally restore superconductivity. The well separated and confined vav-systems could find possible applications as fluxonic devices and might be of use for an advanced control of magnonic excitations in FM/SC systems. In addition, the transport properties for such layered systems depend markedly on the vortex formation. Hence, the current findings could provide additional tools to tune the magnetoresistance in FM/SC multilayers and magnetic tunnel junctions.

Conflict of Interest

The authors declare no conflict of interest.

[1] J. I. Martín, M. Vélez, A. Hoffmann, I. K. Schuller, J. L. Vicent, *Phys. Rev. Lett.* **1991**, *83*, 1022.
[2] M. J. Van Bael, K. Temst, V. V. Moshchalkov, Y. Bruynseraede, *Phys. Rev. B* **1999**, *59*, 14674.
[3] M. Vélez, J. I. Martín, J. E. Villegas, A. Hoffmann, E. M. González, J. L. Vicent, I. K. Schuller, *J. Magn. Magn. Mater.* **2008**, *320*, 2547.
[4] M. V. Milošević, F. M. Peeters, *Phys. Rev. B* **2003**, *68*, 024509.
[5] K. M. D. Hals, *Phys. Rev. B* **2017**, *95*, 134504.
[6] S. S. Pershoguba, K. Björnson, A. M. Black-Schaffer, A. V. Balatsky, *Phys. Rev. Lett.* **2015**, *115*, 116602.
[7] A. Buzdin, *Phys. Rev. Lett.* **2008**, *101*, 107005.
[8] L. A. B. Olde Olthof, X. Montiel, J. W. A. Robinson, A. I. Buzdin, *arXiv*:1907.07510, **2019**.
[9] J. Baumard, J. Cayssol, F. S. Bergeret, A. Buzdin, *Phys. Rev. B* **2019**, *99*, 014511.
[10] K. M. D. Hals, M. Schecter, M. S. Rudner, *Phys. Rev. Lett.* **2016**, *117*, 017001.
[11] S. M. Dahir, A. F. Volkov, I. M. Eremin, *Phys. Rev. Lett.* **2019**, *122*, 097001.
[12] O. V. Dobrovolskiy, R. Sachser, T. Brächer, T. Böttcher, V. V. Kruglyak, R. V. Vovk, V. A. Shklovskij, M. Huth, B. Hillebrands, A. V. Chumak, *Nat. Phys.* **2019**, *15*, 477.
[13] A. A. Bespalov, A. S. Mel'nikov, A. I. Buzdin, *Phys. Rev. B* **2014**, *89*, 054516.
[14] N. I. Polzikova, A. O. Raevskii, *J. Magn. Magn. Mater.* **1995**, *146*, 351.
[15] I. A. Golovchanskiy, N. N. Abramov, V. S. Stolyarov, V. V. Ryazanov, A. A. Golubov, A. V. Ustinov, *J. Appl. Phys.* **2018**, *124*, 233903.
[16] J. S. Neal, M. V. Milošević, S. J. Bending, A. Potenza, L. San Emeterio, C. H. Marrows, *Phys. Rev. Lett.* **2017**, *99*, 127001.
[17] M. V. Milošević, F. M. Peeters, *J. Low Temp. Phys.* **2005**, *139*, 257.
[18] Z. Yang, M. Lange, A. Volodin, R. Szymczak, V. V. Moshchalkov, *Nat. Mater.* **2004**, *3*, 793.
[19] M. Iavarone, S. A. Moore, J. Fedor, S. T. Ciocys, G. Karapetrov, J. Pearson, V. Novosad, S. D. Bader, *Nat. Commun.* **2014**, *5*, 4766.
[20] D. Dew-Hughes, *Low Temp. Phys.* **2001**, *27*, 713.
[21] G. R. Berdiyorov, M. V. Milošević, F. M. Peeters, *Phys. Rev. B* **2006**, *74*, 174512.
[22] E. H. Fyhn, J. Linder, *Phys. Rev. B* **2019**, *100*, 214503.
[23] M. M. Doria, A. D. Romaguera, M. V. Milošević, F. M. Peeters, *EPL* **2007**, *79*, 47006.
[24] R. Rezaev, E. Posenitskiy, E. Smirnova, E. Levchenko, O. G. Schmidt, V. M. Fomin, *Phys. Status Solidi RRL* **2018**, *13*, 1862.
[25] V. M. Fomin, R. O. Rezaev, O. G. Schmidt, *Nano Lett.* **2012**, *12*, 1282.
[26] V. R. Misko, H. J. Zhao, F. M. Peeters, V. Oboznov, S. V. Dubonos, I. V. Grigorieva, *Supercond. Sci. Technol.* **2009**, *22*, 034001.
[27] I. V. Grigorieva, W. Escoffier, V. R. Misko, B. J. Baelus, F. M. Peeters, L. Y. Vinnikov, S. V. Dubonos, *Phys. Rev. Lett.* **2007**, *99*, 147003.
[28] G. Zha, F. M. Peeters, S. Zhou, *EPL* **2014**, *108*, 57001.
[29] A. I. Gubin, K. S. Il'in, S. A. Vitusevich, M. Siegel, N. Klein, *Phys. Rev. B* **2005**, *72*, 064503.
[30] M. Tinkham, *Introduction to Superconductivity*, Courier Corporation, Dover **2004**, p. 454.
[31] M. S. Alnaes, J. Blechta, J. Hake, A. Johansson, B. Kehlet, A. Logg, C. Richardson, J. Ring, M. E. Rognes, G. N. Wells, *Arch. Numer. Software* **2015**, *3*, 2015.
[32] C. Geuzaine, J.-F. Remacle, *Int. J. Numer. Methods Eng.* **2009**, *79*, 1309.
[33] H. Gao, W. Sun, *J. Comput. Phys.* **2015**, *294*, 329.
[34] T. R. Lemberger, Y. L. Loh, *J. Appl. Phys.* **2016**, *120*, 163904.
[35] M. Iavarone, A. Scarfato, F. Bobba, M. Longobardi, G. Karapetrov, V. Novosad, V. Yefremenko, F. Giubileo, A. M. Cucolo, *Phys. Rev. B* **2011**, *84*, 024506.
[36] F. Bobba, C. Di Giorgio, A. Scarfato, M. Longobardi, M. Iavarone, S. A. Moore, G. Karapetrov, V. Novosad, V. Yefremenko, A. M. Cucolo, *Phys. Rev. B* **2014**, *89*, 214502.
[37] M. V. Milošević, G. R. Berdiyorov, F. M. Peeters, *Appl. Phys. Lett.* **2007**, *91*, 212501.